



HAL
open science

Theoretical and Experimental Study for An Improved Cycloid Drive Model

Jean-Luc Dion, Zbigniew Pawelski, Vittorio Chianca, Zbigniew Zdziennicki,
Nicolas Peyret, Grzegorz Uszpolewicz, Janusz Ormezowski, Grzegorz
Mitukiewicz, Xavier Lelasseux

► **To cite this version:**

Jean-Luc Dion, Zbigniew Pawelski, Vittorio Chianca, Zbigniew Zdziennicki, Nicolas Peyret, et al..
Theoretical and Experimental Study for An Improved Cycloid Drive Model. *Journal of Applied
Mechanics*, 2020, 87 (1), 10.1115/1.4044456 . hal-03182247

HAL Id: hal-03182247

<https://hal.science/hal-03182247>

Submitted on 27 Sep 2022

HAL is a multi-disciplinary open access archive for the deposit and dissemination of scientific research documents, whether they are published or not. The documents may come from teaching and research institutions in France or abroad, or from public or private research centers.

L'archive ouverte pluridisciplinaire **HAL**, est destinée au dépôt et à la diffusion de documents scientifiques de niveau recherche, publiés ou non, émanant des établissements d'enseignement et de recherche français ou étrangers, des laboratoires publics ou privés.



Distributed under a Creative Commons Attribution - NonCommercial 4.0 International License

Theoretical and Experimental Study for An Improved Cycloid Drive Model

Jean-Luc Dion

Laboratory Quartz EA7393, SUPMECA Paris-3, Rue Fernand Hainaut, F-93407 Saint Ouen, France

Zbigniew Pawelski

Department of Vehicles and Fundamentals of Machine Design, Lodz University of Technology, ul. Żeromskiego 116, 90-924 Łódź, Poland

Vittorio Chianca

Laboratory Quartz EA7393, SUPMECA Paris-3, Rue Fernand Hainaut, F-93407 Saint Ouen, France

Zbigniew Zdziennicki

Department of Vehicles and Fundamentals of Machine Design, Lodz University of Technology, ul. Żeromskiego 116, 90-924 Łódź, Poland

Nicolas Peyret

Laboratory Quartz EA7393, SUPMECA Paris-3, Rue Fernand Hainaut, F-93407 Saint Ouen, France

Grzegorz Uszpolewicz

Department of Vehicles and Fundamentals of Machine Design, Lodz University of Technology, ul. Żeromskiego 116, 90-924 Łódź, Poland

Janusz Ormezowski

Department of Vehicles and Fundamentals of Machine Design, Lodz University of Technology, ul. Żeromskiego 116, 90-924 Łódź, Poland

Grzegorz Mitukiewicz

Department of Vehicles and Fundamentals of Machine Design, Lodz University of Technology, ul. Żeromskiego 116, 90-924 Łódź, Poland

Xavier Lelasseux

PSA Groupe, 18 Rue des Fauvelles, 92256 La Garenne Colombes, France

This paper describes an experimental and theoretical approach to evaluate cycloid drive reducer efficiency. The tests are carried out on 7.5 kW two-disc cycloid drive with a gear ratio of 19. The torque and speed are measured on the input and output shaft. The efficiency is calculated based on the obtained results. The main goal of the second part of the study is to deduce equations of cycloid reducer in order to predict and analyze experimental results. In this way, the following points are set for the simulation: a working condition in which the input speed and the output load are imposed; then, the output speed is determined by the gear ratio, and finally, the input torque is obtained by solving the dynamic problem. A new model for cycloidal reducers is proposed. This model is based on kinematics and dynamics of rigid bodies and a non-linear stiffness based on contact dynamics. The overall elasticity effects are all condensed between the input shaft and the cycloidal disk. The proposed model allows to predict the efficiency for several operational conditions and offer a drastic reduction of computational costs suitable for the optimization process.

Keywords: multibody analysis, cycloid gearbox, cycloid drive, cycloidal reducer's efficiency, computational mechanics, vibration

1 Introduction

This study is performed with the support of PSA automotive in the technical context of electric car development. Compactness, high-speed range are important benefits of this technology. In this work, we highlight some possible ways to optimize the efficiency of the cycloidal drive. The cycloidal drive, through the important experimentation made during the last years and the new interest in applications, shows relevant operating properties such as long and reliable working life, large range of gear ratio in comparison with the traditional gearboxes. If it is well designed, it displays minimal vibrations and low noise, high overload capacity, reverse applications as a reducer, high efficiency with increasing load and compact design. All these reasons encourage both the experimentation and the computational work with the main purpose of finding the pivotal features to increase the efficiency. Most research studies aim to perform a better knowledge of cycloidal drive, predict important factor such as efficiency and perform new designs. Mackic et al. [1] investigate the influence of geometrical parameters on the cycloid drive efficiency. They summarize that the optimum choice of design parameters has a significant impact on its efficiency. Blagojevic et al. [2] developed a model of cycloid drive which only takes into account the friction in contact of the cycloid disk and housing rollers, while the occurrence of friction in other locations is neglected. They notice that the appearance of friction has a significant impact on the core strength parameter of the cycloidal speed reducer. In another paper, Blagojevic et al. [3] introduce a dynamic model of the cycloid drive which takes into consideration the elastic connection with stiffness and damping between the bodies in contact: between the input shaft and the eccentric cam (cycloidal plate), between the housing roller and the cycloidal plate, between the output rollers and the cycloidal plate. The simulations show that the biggest influence on operating condition of the cycloid drive comes from the damping and stiffness in the contact between the cycloid gear tooth and the housing pin. Moreover, the kinematics is inspired by Shin and Kwon [4]. These authors apply the Kennedy theorem on the cycloidal disk in order to analyze its kinematics. Some papers develop the technological context of specific applications for cycloidal reducers:

contact analysis in Refs. [5–8], geometric assessments in Refs. [9–12]. The present study is developed from tests of the cycloid drive device (Sec. 2) on a test bench designed at AML (Sec. 3) with a specific measurement methodology (Sec. 4). Then, a new method for cycloid drive analysis is introduced with equations deduced in order to predict and analyze experimental results made on the same device (Sec. 5). A non-linear model based on contact dynamics is proposed in Sec. 5 for the overall elastic force. Simulation results are described (Sec. 6) and pointed out regarding tests for the conclusion (Sec. 7). In accordance with previous works performed in Refs. [13,14], this article assumes that the efficiency depends on the input torque: the architecture and the geometry plays a major role in the reducer performance. In order to improve the efficiency, the dynamics had to be investigated more. As demonstrated in Ref. [15], even for complete rigid bodies (without any elasticity), the efficiency strongly depends on the eccentricity between the input shaft and cycloidal plate. In this way, smaller is the eccentricity, smaller is the dynamics of the gap between the pins and the cycloid teeth. From this article’s point of view, this is due to non-linear dynamic effects when stiffness increases with the load.

2 Research Object

The tested machine has been designed for this research study and is composed of two disks (Fig. 1). Each disk has 19 teeth (z_1) and cooperates with housing equipped with 20 housing pins (z_2). In this case, the total ratio of the gearbox is

$$i = \frac{\omega_{in}}{\omega_{out}} = \frac{-z_1}{z_2 - z_1} = -19 \quad (1)$$

The main nominal values of the cycloidal reducer are presented in the following table:

Rotational speed of input shaft	1500	rpm
Power	7.5	kW
Gear box ratio	19	–

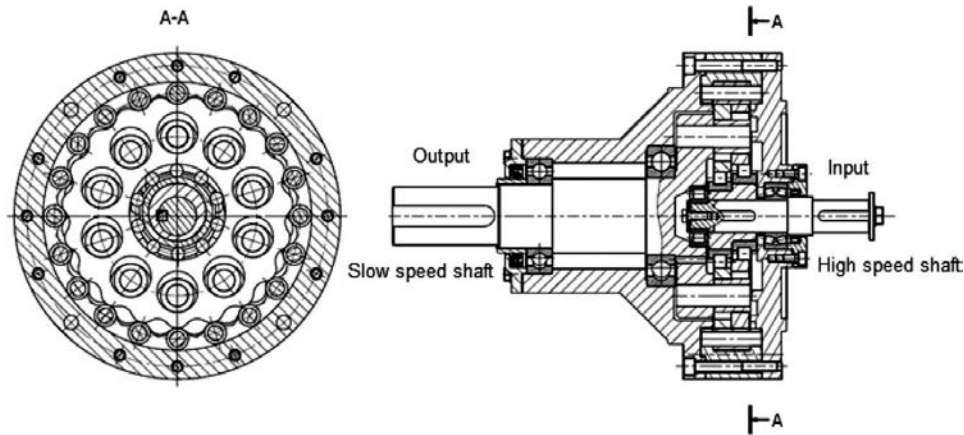


Fig. 1 Two sections of the cycloidal gearbox, $z_1 = 19$ teeth and $z_2 = 20$ housing pins, ω_{in} on the small shaft (high speed on the right side), and ω_{out} on the big shaft (low speed on the left side). This new design introduces specific brass washers in order to reduce friction forces and improve efficiency.

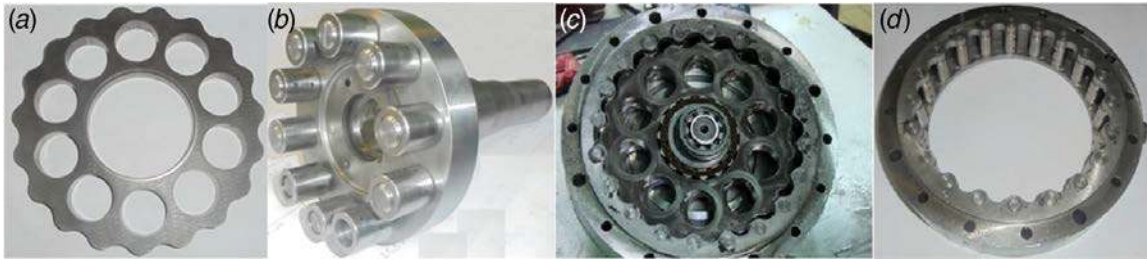


Fig. 2 Tested cycloidal drive: (a) cycloidal plate, (b) output shaft and output rollers, (c) cyclo gearbox, and (d) housing with pins

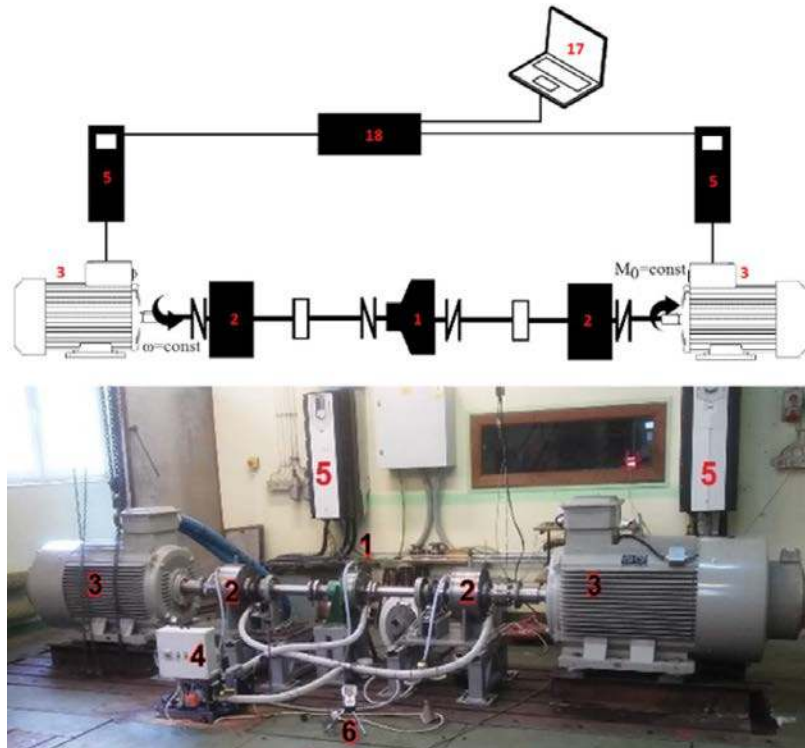


Fig. 3 Test bench schematic view: 1, cycloidal gearbox; 2, planetary gear set; 3, electric motor; 4, oil supply system; 5, inverter; 6, sound meter; 17, computer with an application software tool for the inverter control system; and 18, inverter control system

The parts of the new cycloid gearbox were manufactured in Lodz (Fig. 2).

3 Test Bench

The cycloidal gearbox was tested on the bench assembled at AML (Fig. 3).

The test bench consists of the following:

- (1) Two electrical motors “3” (200 kW each), which are characterized by reversible work, they can operate both as a motor or as a break. The common DC voltage cable allows the transmission of electrical energy from the generator to the engine. In this way, the external power supply is charged only to cover energy losses much smaller than appear in the working drive system.
- (2) Inverters “5” are made by two ABB frequency converters, which in the power supply have a rectifier bridge and an input filter in order to reduce harmonic distortion from the external power supply.
- (3) The CPU “17” (Fig. 3) allows to plan and to execute the experiment. Experimental cycle of electrical machines can be carried out with step, trapezoidal, or sinusoidal function.

- (4) An oil cooling system is used to keep the desired temperature inside the cyclo gearbox’s housing.
- (5) The oil temperature sensor is mounted at the bottom of the cycloid gear housing. It allows the observation of oil average temperature during bench operation.

In order to reduce the vibration of test components, a set of laser sensors “ShaftAlign” made by Prüftechnik was used to set coaxiality for shafts and clutches in the drive line. After reaching the required accuracy in setting the cooperating connections, the test can be started. The control system “18” allows to set up the speed on the input shaft and the torque on the output shaft. Thus, the system keeps the speed constant when the torque increases at the braking side. In the same way, the system keeps the torque constant on the braking unit when the speed increases at the input side. In transient conditions, the torque and speed can vary due to the moment of inertia. The measurement system consists of the following:

- (1) Two torque and speed sensors HBM T40b, which are mounted on the input and output shaft of the cycloidal gearbox.
- (2) Temperature sensor that measures the oil temperature in the gearbox.

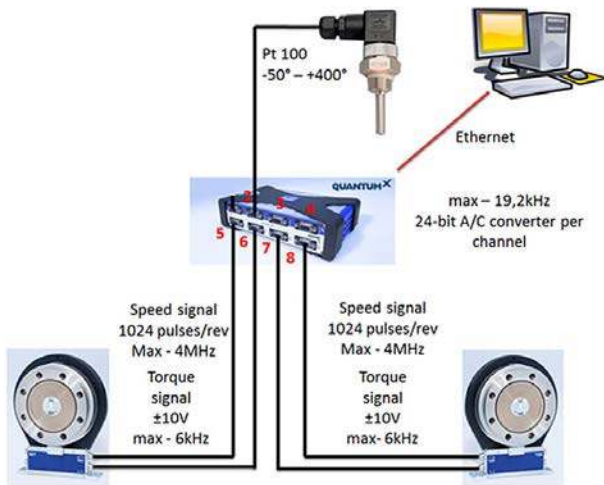


Fig. 4 Data acquisition system

A schematic view of the data acquisition hardware is shown in Fig. 4.

4 Methodology and Results

Tests are carried out at constant torques on the output shaft of the tested gear. The speed increased from 0 rpm to the set maximum value kept constant during 20 s and then decreased to 0 rpm again (maximum value kept for input speed as equal to 2200 rpm). Example of the acquired data is shown in Fig. 5; as it may be observed that there are no important oscillations during the 20 s; moreover, during that time, the data of efficiency will be taken.

The torques and speed values acquired during these 20 s are averaged. The instantaneous efficiency is computed according to the formula:

$$\eta = \frac{T_{out} \omega_{out}}{T_{in} \omega_{in}} \quad (2)$$

As we can see by the trend of efficiency in Fig. 5, the system reaches quickly the stationary condition referring to the transmission

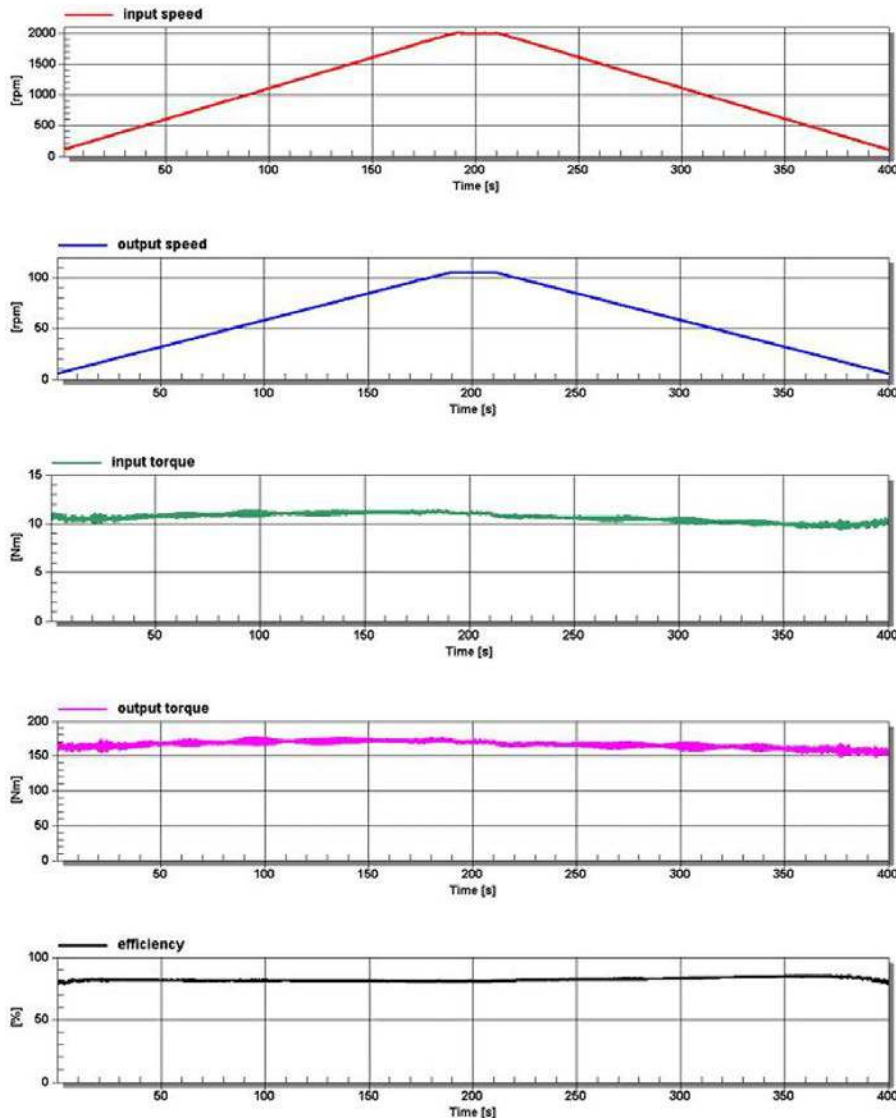


Fig. 5 A sample of measured signals

efficiency, this is one of the main reason why, in a latter time, we impose stationary working conditions on dynamics.

The oil temperature was kept around 33 °C in order to have a quite constant oil viscosity around 44 mm²/s to avoid the influence of a variation of this environmental parameter.

The main efficiency results obtained with the test bench are summarized in Fig. 6. there is a relevant dependence of efficiency on output torque, while the input speed does not significantly affect the efficiency especially for high values of the load.

5 Dynamics Model

5.1 Kinematic Analysis. First, the gearbox ratio of the cycloid drive (Fig. 7) is obtained by using the Willis formula in the case of having the ring in a fixed state:

$$i = \frac{\omega_{in}}{\omega_{out}} = \frac{-z_1}{z_2 - z_1} \quad (3)$$

For compactness and efficiency reasons, most of the cycloid drive is designed with $z_2 = z_1 + 1$; then, the gearbox ratio is $i = z_1$.

Following formula are based on the theorem of Kennedy. The theorem of Kennedy states that the three instantaneous centers of

rotation shared by three rigid bodies in relative planar motion (whether or not connected) all lie on the same straight line. Figure 8 shows the geometric outline: part 1 (housing pin) is in contact with part 3 (cycloidal plate) and part 3 (cycloidal plate) is in contact with part 2 (input shaft). O is the center of rotation of the input shaft and O_1 is the center of the cycloidal disk. The point O is the instant center of rotation of the body 2, so $I_{12} = O$. Moreover, part 3 is in rotation with part 2 in the center O_1 , then the point O_1 is the instant center of rotation of part 3 relatively to part 2: $I_{23} = O_1$. Applying the Kennedy theorem, we obtain the position of I_{31} . In fact, I_{31} is located at the intersection of the straight (OO_1) and the normal to the tangent at the point of contact A between the cycloidal disc and housing pin. The velocity of the point O_1 is obtained with the theorem of Rival applied in the instant center of rotation I_{31} :

$$\vec{V}_{O_1 \in 2/1} = \vec{\omega}_{2/1} \times \vec{OO}_1 \quad (4)$$

$$\vec{V}_{O_1 \in 3/1} = \vec{\omega}_{3/1} \times \vec{I_{31}O_1} \quad (5)$$

$\vec{V}_{O_1 \in 2/1}$ is the speed of point O_1 inbuilt to part 2 relatively to part 1, $\vec{V}_{O_1 \in 3/1}$ is the speed of point O_1 inbuilt to part 3 relatively to part 1

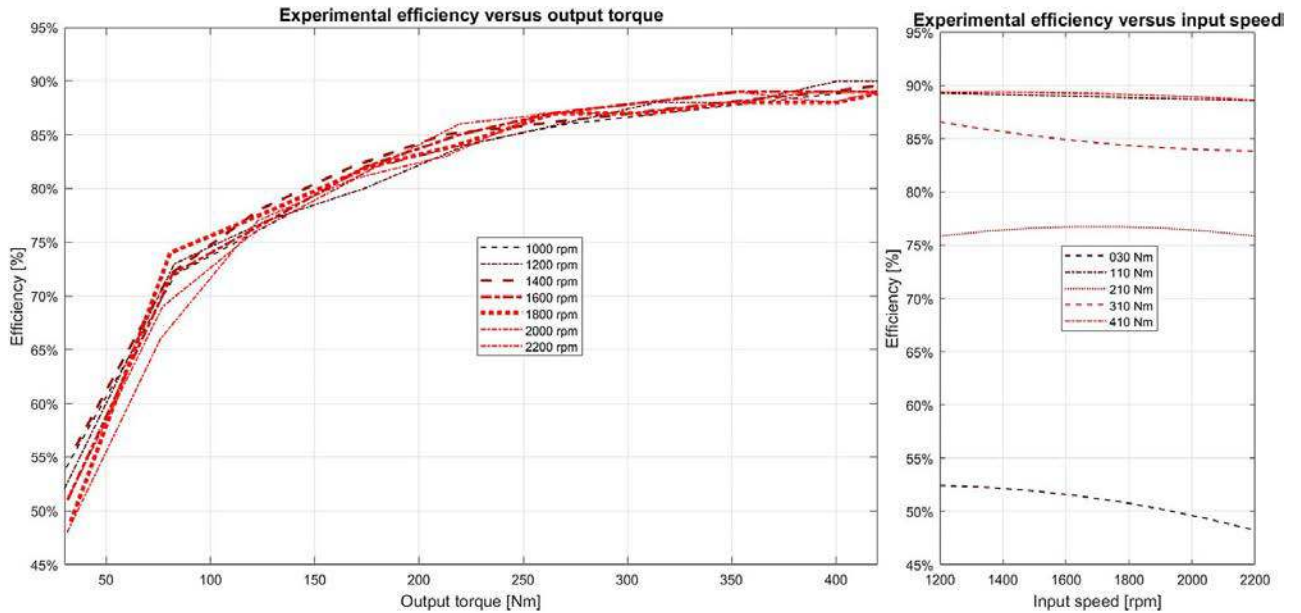


Fig. 6 Computed efficiency versus torque for several speeds and versus speed for several values of load (examples of data are in Appendix B)

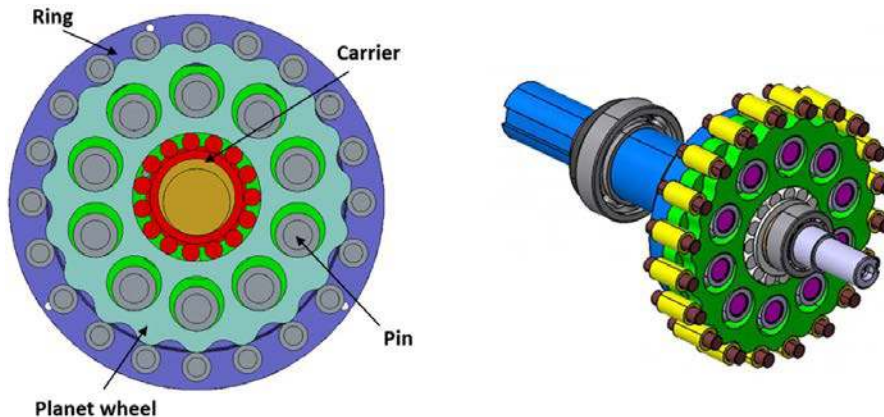


Fig. 7 CAD model of the reduce

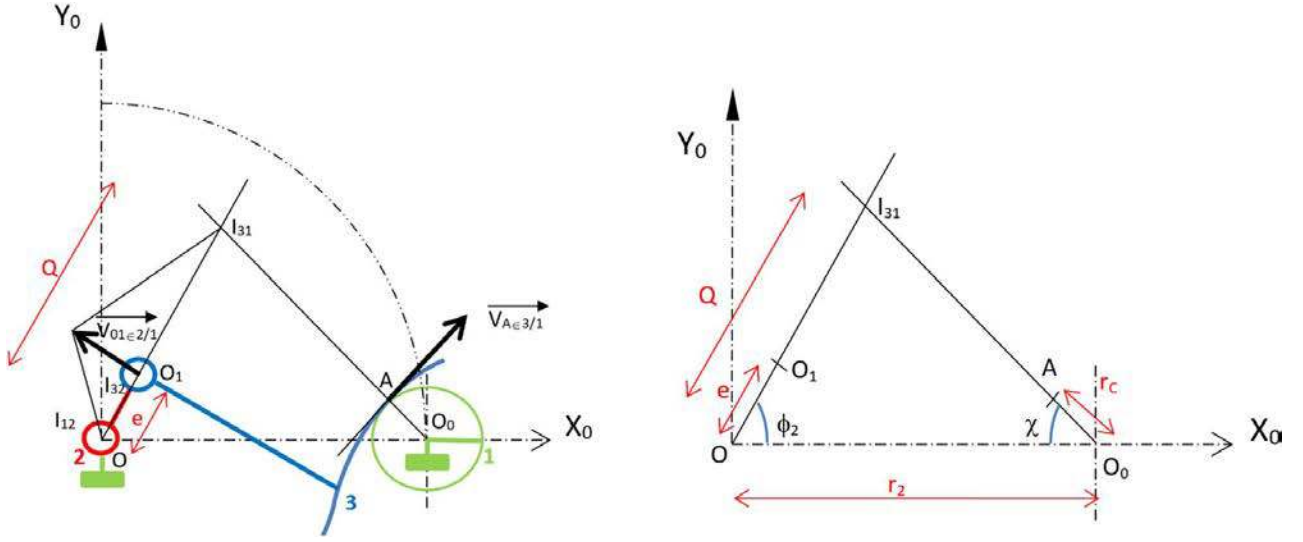


Fig. 8 Geometric setup of the cycloidal disc with a contact point A (between cycloidal disc and a single housing pin): 1, housing pin; 2, input shaft; and 3, cycloidal plate

and leads to

$$\overrightarrow{V_{O_1 \in 2/1}} = \overrightarrow{V_{O_1 \in 3/1}} \quad (6)$$

Thus,

$$\frac{\omega_{3/1}}{\omega_{2/1}} = -\frac{e}{Q-e} \quad (7)$$

where e is the eccentricity between the axis of the input shaft and the axis of the cycloidal disc (the floating clearance with continuous contact). Q is the length of the segment $I_{31}O_1$, and $\omega_{2/1}$ is the input speed of the mechanism. The contact between the internal lobes of the cycloidal disk and the output rollers inbuilt to the output shaft is homo-kinetic. The angular speeds of the cycloidal disk and the output shaft are equal. $\omega_{3/1}$ is the output speed. Knowing $\omega_{3/1}/\omega_{2/1} = (z_2 - z_1)/z_1$, Q is obtained:

$$Q = \frac{z_2 e}{z_2 - z_1} \quad (8)$$

Point A belongs to line $I_{31}O_0$ with a distance from O_0 equal to the radius of housing pins r_c . r_2 is the distribution radius of the housing pins. The position of point A referring to Fig. 8 is given by

$$\begin{cases} X_A = r_2 - r_c \cos \chi \\ Y_A = r_c \sin \chi \end{cases} \quad (9)$$

And, χ is built from geometric properties in Fig. 8:

$$\chi = \arctan\left(\frac{Q \sin \phi_2}{r_2 - Q \cos \phi_2}\right) = \arctan\left(\frac{\sin \phi_2}{r_2/Q - \cos \phi_2}\right) \quad (10)$$

For the consecutive works on dynamics, it is relevant to know the velocity of the contact point A:

$$\overrightarrow{V_{A \in 3/1}} = \overrightarrow{\omega_{3/1}} \times \overrightarrow{I_{31}A} \quad (11)$$

knowing:

$$\overrightarrow{I_{31}A} = \begin{bmatrix} r_2 - r_c \cos \chi - Q \cos \phi_2 \\ r_c \sin \chi - Q \sin \phi_2 \\ 0 \end{bmatrix} \quad (12)$$

When the previous term is developed:

$$\overrightarrow{I_{31}A} = \begin{bmatrix} r_2 - r_c \frac{r_2 - \cos \phi_2}{\sqrt{\frac{r_2}{Q} - 2 \cos \phi_2}} - Q \cos \phi_2 \\ \sqrt{\frac{r_2}{Q} - 2 \cos \phi_2} \\ r_c \frac{\sin \phi_2}{\sqrt{\frac{r_2}{Q} - 2 \cos \phi_2}} - Q \sin \phi_2 \\ 0 \end{bmatrix} \quad (13)$$

The velocity of the point A becomes

$$\overrightarrow{V_{A \in 3/1}} = \overrightarrow{\omega_{3/1}} \times \overrightarrow{I_{31}A} = \begin{bmatrix} \omega_{3/1} \left(r_c \frac{\sin \phi_2}{\sqrt{\frac{r_2}{Q} - 2 \cos \phi_2}} - Q \sin \phi_2 \right) \\ -\omega_{3/1} \left(r_2 - r_c \frac{r_2 - \cos \phi_2}{\sqrt{\frac{r_2}{Q} - 2 \cos \phi_2}} - Q \cos \phi_2 \right) \\ 0 \end{bmatrix} \quad (14)$$

Based on these results, the complete kinematics of the reducer is known and lay the foundations to solve the dynamics.

5.2 Analytic Formulations of Forces. In order to apply the fundamental law of dynamics, the forces acting upon the cycloidal disk are defined:

- The force (normal E_x and tangential components $(1 - \mu_E)E_y$) (center of Fig. 9) applied on the cycloidal disk by the input shaft (through the intermediate bearing).
- The forces (normal $F_{N,i}$ and tangential components $\mu_p F_{N,i}$) applied on the cycloidal disk by the housing pins in contact.
- The forces (normal $F_{k,j}$ and tangential components $\mu_s F_{k,j}$) applied on the cycloidal disk by the output rollers.

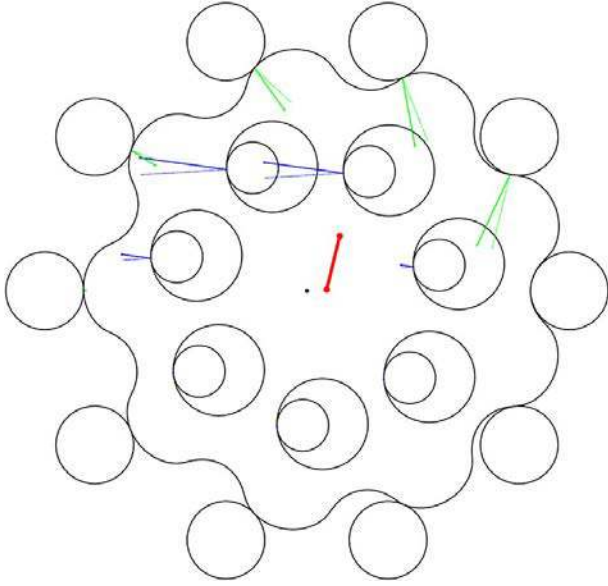


Fig. 9 Sketch of the cycloid drive and forces acting on the cycloidal disk

The retained assumptions are as follows:

- The output torque is constant.
- All the bodies are rigid, no deformations are taken into account in this model (rigid bodies model).
- Input speed is constant and output speed obtained from the gear ratio;
- Input torque is unknown and obtained by solving the dynamic problem;
- Only one disc is modeled. Experimentation (made in Lodz) shows that the number of discs does not modify the experimental trend of efficiency. Model is made with only one disc, with the hypothesis that one disc see half of the complete torque of the reducer because two discs are working in parallel. This hypothesis involves that the losses of the two parallel discs should have the same non-linearity behavior and level.

To fit to the experimentation, the disc calculations are made with half-torque of the experimentation torque.

Due to geometry construction, without clearance between disc and pins, all pins can not be loaded all together and simultaneously. Then, at any time, of all the pins, some ones are fully loaded, others partially or not loaded.

$$F_{N,i}(\phi_{2i}) = \begin{cases} F_{max,N} \frac{r_2}{Q} \frac{\sin \phi_{2i}}{\sqrt{1 + \left(\frac{r_2}{Q}\right)^2 - 2\frac{r_2}{Q} \cos \phi_{2i}}} & \text{if } 0 \leq \phi_{2i} \leq \pi \\ 0 & \text{if } \pi \leq \phi_{2i} \leq 2\pi \end{cases} \quad (15)$$

The load distribution linked to the contact between rollers and cycloidal plate is defined as follows (Fig. 10):

$$F_{k,j}(\phi_{2j}) = \begin{cases} F_{max,k} \sin \phi_{2j} & \text{if } 0 \leq \phi_{2j} \leq \pi \\ 0 & \text{if } \pi \leq \phi_{2j} \leq 2\pi \end{cases} \quad (16)$$

5.3 Rigid Bodies Model. The initial model is a rigid bodies model. Therefore, no elastic property is introduced in dynamics. All the numerical values of parameters are resumed in Appendix A. Acting forces do not involve any deformation. Acting forces do not affect the efficiency of the reducer. All the previous equations are the outcome of the hypotheses of rigid bodies. $X_1O_1Y_1$ is the mobile reference system, and X_0OY_0 is the fixed system. The kinematic torsor of the cycloidal plate referring to the X_0OY_0 is

$$\{C_{C_y/R_0}\} = \left\{ -\frac{\dot{\phi}}{z_1} \vec{Z} \mid e\dot{\phi} \vec{Y}_1 \right\}_{X_0OY_0} \quad (17)$$

The dynamic torsor of the cycloidal plate is

$$\{D_{C_y/R_0}\} = \left\{ -m_{cy} e\dot{\phi}^2 \vec{X}_1 + m_{cy} e\ddot{\phi} \vec{Y}_1 \mid -\frac{I_{zz}}{z_1} \ddot{\phi} \vec{Z} \right\}_{X_0OY_0} \quad (18)$$

where m_{cy} is the cycloidal disk's mass and I_{zz} is its moment of inertia.

The main dynamic interactions between the cycloidal disk and the other bodies are given as follows:

- The action of the input shaft on the cycloidal disk:

$$\{E_{C_y/R_0}\} = \left\{ E_x \vec{X}_1 + \text{sgn}(\omega_0)(1 - \mu_E) E_y \vec{Y}_1 \mid (1 - \mu_E) E_y e \vec{Z} \right\}_{X_0OY_0} \quad (19)$$

- The action of the housing pins on the cycloidal disk:

$$\{O_{C_y/R_0}\} = \left\{ \vec{C}_{O_i} = K_c \sum_i C_{X_i} \vec{X}_1 + K_c \sum_i C_{Y_i} \vec{Y}_1 \mid \sum_i (\vec{O} \vec{A}_i \times \vec{C}_{O_i}) \right\}_{X_0OY_0} \quad (20)$$

$$\{O_{C_y/R_0}\} = \left\{ \vec{C}_{O_i} = K_c \sum_i C_{X_i} \vec{X}_1 + K_c \sum_i C_{Y_i} \vec{Y}_1 \mid \sum_i K_c M_{C_i} \vec{Z} \right\}_{X_0OY_0} \quad (21)$$

where i stays for the i th pin in contact with the plate.

- The action of the output rollers on the cycloidal disk:

$$\{O_{S_y/R_0}\} = \left\{ \vec{S}_{O_j} = K_s \sum_j S_{X_j} \vec{X}_1 + K_s \sum_j S_{Y_j} \vec{Y}_1 \mid \sum_j (K_s \vec{O} \vec{S}_j \times \vec{S}_{O_j}) \right\}_{X_0OY_0} \quad (22)$$

$$\{O_{S_y/R_0}\} = \left\{ \vec{S}_{O_j} = K_s \sum_j S_{X_j} \vec{X}_1 + K_s \mu_s \sum_j S_{Y_j} \vec{Y}_1 \mid K_s \sum_i M_{S_j} \vec{Z} \right\}_{X_0OY_0} \quad (23)$$

where j stays for the j th roller in contact with the plate.

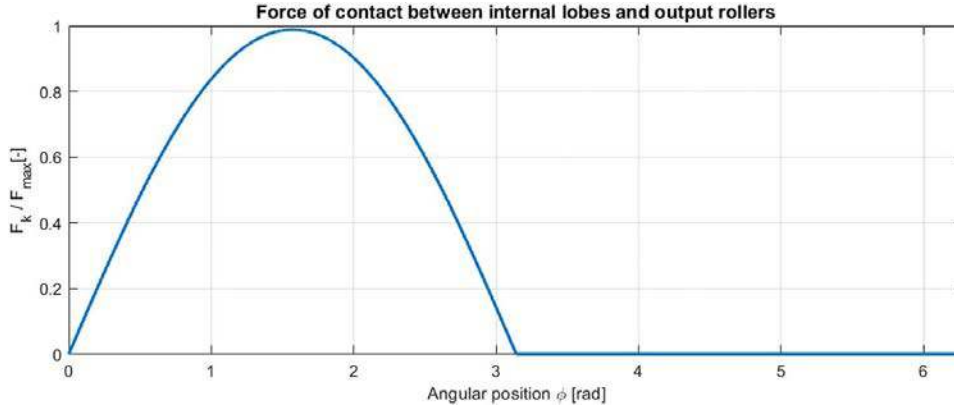


Fig. 10 Contacting force during the engagement

In the main equations, there are two coefficients K_c and K_s that are strictly linked to the maximum values of the forces exchanged. K_s is obtained by the balance on the output shaft. K_c is an unknown parameter identified by solving the dynamic problem. The terms inside the sums are tied to the geometrical distribution of forces.

Then, we apply the fundamental principle of the dynamics with the virtual work principle. The cycloidal disc is a rigid body moving into a plane. It involves three degrees of freedom in the general case.

Along the \vec{X}_1 direction:

$$\sum (\vec{F} \cdot \delta \vec{X}_1) = 0; \quad K_c \sum_i C_{X_i} + K_s \sum_j S_{X_j} + E_x + m_{cy} e \dot{\varphi}^2 = 0 \quad (24)$$

Along the \vec{Y}_1 direction:

$$\sum (\vec{F} \cdot \delta \vec{Y}_1) = 0; \quad K_c \sum_i C_{Y_i} + K_s \mu_s \sum_j S_{X_j} + E_y (1 - \mu_E) - m_{cy} e \ddot{\varphi} = 0 \quad (25)$$

Regarding the balance of torques around the axis \vec{Z} :

$$\sum (\vec{M}_Z \cdot \delta \vec{\theta}_Z) = 0; \quad K_c \sum_i M_{C_i} + K_s \sum_j M_{S_j} + E_y e (1 - \mu_E) + \frac{I_{zz}}{z_1} \ddot{\varphi} = 0 \quad (26)$$

Unknown variables in the dynamic problem are as follows: E_x , E_y , K_c , K_s , φ and its first and second derivatives. The balance of torque on the output shaft leads to

$$K_s \sum_i M_{S_j} \vec{Z} - \frac{I_{zzos}}{z_1} \ddot{\varphi} \vec{Z} - C_s \vec{Z} = 0 \quad (27)$$

where I_{zzos} is the moment of inertia of the output shaft and C_s is the constant output load imposed on the output shaft. Then,

$$\begin{cases} K_c \sum_i C_{X_i} + K_s \sum_j S_{X_j} + E_x + m_{cy} e \dot{\varphi}^2 = 0 \\ K_c \sum_i C_{Y_i} + K_s \mu_s \sum_j S_{X_j} + E_y (1 - \mu_E) - m_{cy} e \ddot{\varphi} = 0 \\ K_c \sum_i M_{C_i} + K_s \sum_j M_{S_j} + E_y e (1 - \mu_E) + \frac{I_{zz}}{z_1} \ddot{\varphi} = 0 \\ K_s \sum_j M_{S_j} - \frac{I_{zzos}}{z_1} \ddot{\varphi} - C_s = 0 \end{cases} \quad (28)$$

Considering the steady state of the system:

$$\ddot{\varphi}(t) = 0, \quad \dot{\varphi}(t) = \omega_0 \quad (29)$$

And the system of equations becomes

$$\begin{cases} K_c \sum_i C_{X_i} + K_s \sum_j S_{X_j} + E_x + m_{cy} e \omega_0^2 = 0 \\ K_c \sum_i C_{Y_i} + K_s \mu_s \sum_j S_{X_j} + E_y (1 - \mu_E) = 0 \\ K_c \sum_i M_{C_i} + K_s \sum_j M_{S_j} + E_y e (1 - \mu_E) = 0 \\ K_s \sum_j M_{S_j} - C_s = 0 \end{cases} \quad (30)$$

Regarding unknown variables K_c , E_x , and E_y , the system is expressed in a matrix way as follows:

$$\begin{pmatrix} \sum_i C_{X_i} & 1 & 0 \\ \sum_i C_{Y_i} & 0 & 1 - \mu_E \\ \sum_i M_{C_i} & 0 & (1 - \mu_E)e \end{pmatrix} \begin{bmatrix} K_c \\ E_x \\ E_y \end{bmatrix} = \begin{bmatrix} -m_{cy} e \omega_0^2 - K_s \sum_j S_{X_j} \\ -K_s \mu_s \sum_j S_{X_j} \\ K_s \sum_j M_{S_j} \end{bmatrix} \quad (31)$$

Analytic solution leads to

$$T_{in} = E_y (1 - \mu_E) e = K_s e \frac{\sum_i C_{Y_i} \sum_j M_{S_j} + \mu_s \sum_j S_{X_j} \sum_i M_{C_i}}{\sum_i C_{Y_i} e - \sum_i M_{C_i}} \quad (32)$$

And the instantaneous efficiency of gearbox transmission is defined by

$$\eta = \frac{T_{out} \omega_{out}}{T_{in} \omega_{in}} = \frac{\sum_j M_{S_j} (\sum_i C_{Y_i} e - \sum_i M_{C_i})}{e z_1 (\sum_i C_{Y_i} \sum_j M_{S_j} + \mu_s \sum_j S_{X_j} \sum_i M_{C_i})} \quad (33)$$

In order to simulate the system in working condition, the input speed and the output load are imposed. The output speed is determined by the gear ratio and the input torque is obtained by solving the dynamic problem. This operating condition is comparable with the working state of the test's bench. However, as Eq. (33) shows, due to the hypothesis of rigid bodies, the efficiency does not depend on the constant output load (represented by K_s). For this main reason, we improve our model in the following section.

5.4 Stiffness Model. In order to model the stiffness of parts in contact, several studies have been performed. LiXin Xu and YuHu Yang [16] propose a detailed model based finite element method (FEM) for the design of the bearings; Hsieh [17] in a same approach focuses on pinwheel and its effect on efficiency. The contact dynamics is analyzed in Refs. [18,19] in order to predict dynamics and local stress effects. The studies on paper [15] propose in a similar way a study on a large set of parameters with a specific study on each parameter and its effects on efficiency.

These studies are based on FEM with detailed models designed to predict, torques, loads, and stress on several parts. In order to compute the efficiency (the ratio between instantaneous powers between input and output shaft), all applied loads and torques

have to be defined and computed on the input shaft and the output shaft. In the tested conditions (see Sec. 4) with controlled output conditions, all the dynamics due to the stiffness of parts in contact can be condensed on the input shaft.

In that way, the reduced-order model of a cycloid drive, taking into account the equivalent static behavior and the first non-linear mode, can be produced with an equivalent non-linear stiffness condensed between the input shaft and the cycloidal disc. According these assumptions and objectives, a mobility with stiffness is introduced along the direction of force transmission between the input shaft and the cycloidal disc. The main properties of these mobility and stiffness depend on the following:

- The capability to take into account the overall elastic effects on dynamics.
- The eccentric bearing, in a first approximation, is included as being inbuilt in the input shaft. In contact dynamics, the elastic relationship between force and deformation in contacts is non-linear.
- Because of the small axial length of the disk, its contact with the input shaft can not be assumed as a contact between cylinders of infinite length, neither as the contact between two spheres.

- The mobility and elasticity introduced only between the input shaft and cycloidal disc are the direct consequence of previous works, the focus of which is the analysis of strength and stress distribution (see Ref. [3]). The most stressed sections of the cycloidal plate are those closer to the coupling with the input shaft in the direction of the force (\vec{Y}_1). Thus, the main elastic effects involve in this mechanical joint (Fig. 11).

In the following model, the elastic force is non-linear and k_{cy} is the non-linear stiffness coefficient and p is the exponent of non-linearity. Then, the relation is linear only in the case of $p = 1$.

$$\overrightarrow{F_{el}(y_1)} = -k_{cy}|y_1|^p \frac{y_1}{|y_1|} \vec{Y}_1 = -k_{cy}y_1|y_1|^{p-1} \vec{Y}_1 \quad (34)$$

The kinematic torsor of the cycloidal disc is as follows:

$$\{C_{C_y/R_0}\} = \left\{ -\frac{\dot{\varphi}}{z_1} \vec{Z} |e\dot{\varphi}\vec{Y}_1 + (\dot{y}_1\vec{Y}_1 - y_1\dot{\varphi}\vec{X}_1) \right\}_{X_0OY_0} \quad (35)$$

The kinematics used is the same as the previous model, and displacements along y_1 are assumed as small displacements. Thanks to the kinematic torsor, the dynamic torsor of the cycloidal disc is written as follows:

$$\{D_{C_y/R_0}\} = \left\{ m_{cy}(-e\dot{\varphi}^2 - 2\dot{y}_1\dot{\varphi} - \ddot{y}_1)\vec{X}_1 + m_{cy}(e\ddot{\varphi} + \ddot{y}_1 - y_1\dot{\varphi}^2)\vec{Y}_1 - \frac{I_{zz}}{z_1}\ddot{\varphi}\vec{Z} \right\}_{X_0OY_0} \quad (36)$$

The torsor representing the interactions between the input shaft and the cycloidal disc is defined as follows:

$$\{E_{C_y/R_0}\} = \left\{ E_x\vec{X}_1 - k_{cy}y_1|y_1|^{p-1}\vec{Y}_1 - k_{cy}y_1|y_1|^{p-1}e\vec{Z} \right\}_{X_0OY_0} \quad (37)$$

Along the \vec{X}_1 :

$$\sum(\vec{F} \cdot \delta\vec{X}_1) = 0; \quad K_c \sum_i C_{X_i} + K_s \sum_j S_{X_j} + E_x + m_{cy}(e\dot{\varphi}^2 + 2\dot{y}_1\dot{\varphi} + \ddot{y}_1) = 0 \quad (38)$$

Along the \vec{Y}_1 :

$$\sum(\vec{F} \cdot \delta\vec{Y}_1) = 0; \quad K_c \sum_i C_{y_i} + K_s \mu_s \sum_j S_{X_j} - k_{cy}y_1|y_1|^{p-1} + m_{cy}(-e\ddot{\varphi} + \ddot{y}_1 - y_1\dot{\varphi}^2) = 0 \quad (39)$$

Regarding the balance of torque around the axis \vec{Z} :

$$\sum(\vec{M}_Z \cdot \delta\theta_Z) = 0; \quad K_c \sum_i M_{C_i} + K_s \sum_j M_{S_j} - ek_{cy}y_1|y_1|^{p-1} + \frac{I_{zz}}{z_1}\ddot{\varphi} = 0 \quad (40)$$

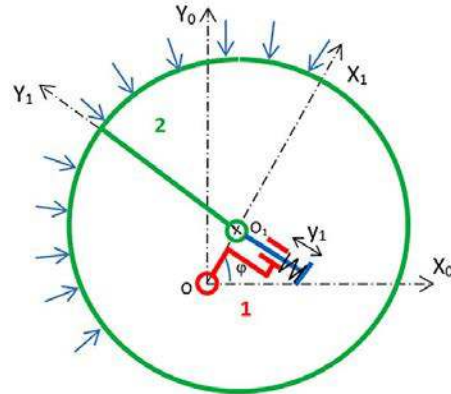
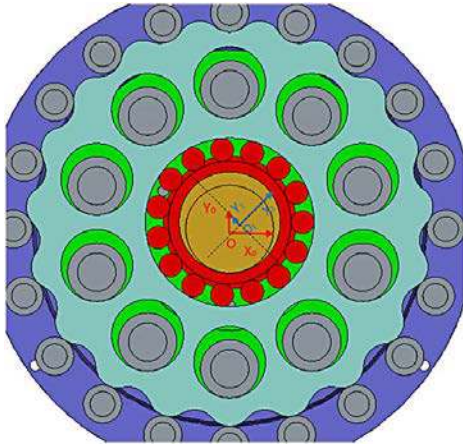


Fig. 11 Model for y_1 mobility introducing a contact stiffness: part 1 represents the input shaft, part 2 represents the cycloidal disc's internal coupling surface (O_1 is the cycloidal disc's center and O is the input shaft's center)

Then, by using Eqs. (39) and (40) and steady-state assumption ($\dot{\varphi} = 0$ and $\dot{\varphi} = \omega_0$), the system of equations is defined as follows:

$$\begin{cases} K_c \sum_i M_{C_i} + K_s \sum_j M_{S_j} - k_{cy} e |y_1|^{p-1} y_1 = 0 \\ K_c \sum_i C_{Y_i} + K_s \mu_s \sum_j S_{X_j} - k_{cy} |y_1|^{p-1} y_1 + m_{cy} (\ddot{y}_1 - y_1 \omega_0^2) = 0 \end{cases} \quad (41)$$

K_c can be expressed as a function of y_1 from the first equation of the system (41):

$$K_c = \frac{-K_s \sum_j M_{S_j} + k_{cy} e |y_1|^{p-1} y_1}{\sum_i M_{C_i}} \quad (42)$$

by substituting K_c in the second equation of Eq. (41), we obtain:

$$\begin{aligned} m_{cy} \ddot{y}_1 + k_{cy} y_1 |y_1|^{p-1} \left(1 - e \frac{\sum_i C_{Y_i}}{\sum_i M_{C_i}} \right) - m_{cy} \omega_0^2 y_1 \\ = K_s \mu_s \sum_j S_{X_j} - K_s \sum_j M_{S_j} \frac{\sum_i C_{Y_i}}{\sum_i M_{C_i}} \end{aligned} \quad (43)$$

The equation above is a non-linear differential equation with terms varying over time, the solution of which is determined numerically by using a step-by-step solver. With these numerical results, the efficiency of the gearbox transmission is computed. For a steady state (and without dynamic effects), the efficiency is defined as follows:

$$\eta = \frac{T_{out} \omega_{out}}{T_{in} \omega_{in}} = \frac{C_S}{z_1 e k_{cy} |y_1|^p} \quad (44)$$

The main idea of introducing the solution only in steady state is from the assumption to describe the dynamic behavior under nominal steady-state conditions: we have observed the reduced transitional phase until reaching the nominal working conditions. Thanks to the torque balance on the input shaft, we obtain the following equation:

$$T_{in} = [\overrightarrow{F_{el}(y_1)} \times (e \overrightarrow{X_1})] \cdot \overrightarrow{Z} = k_{cy} |y_1|^p e \quad (45)$$

C_S is the output load and e is the eccentricity between the axes of the input shaft and the cycloidal disk, thus $\frac{\omega_{in}}{\omega_{out}} = z_1$.

6 Results From Computational Simulations

This section focuses on some details of simulations and the main results from the mathematical model proposed. The forces and the solution of the dynamic problem are computed with MATLAB, the differential equation with the stiffness model is solved with SIMULINK. Only steady states are studied, transient responses from starting point are rejected in all the presented analysis. The first model that we have used to evaluate the efficiency of the reducer is the rigid bodies model. The dynamics of forces exchanged is made very clear by using this rigid bodies model (Fig. 12).

However, even if the rigid bodies model fully explains the dynamics of the forces exchanged between all the bodies, the forecast of the efficiency is poor and does not respect the trends observed experimentally.

According to the rigid bodies model, the efficiency does not depend on the input speed and the output load, the only dependence is for the geometrical parameters of the machine and we can discover that by simulating this model on MATLAB.

First, the improved model (with the mobility and the stiffness) is computed and its efficiency is evaluated with the parameter p equal to 1 (Fig. 13).

The chosen stiffness model comes from the linearization of contact forces. The computed efficiency does not depend on the input speed (as for the experimentation) and depends too very weakly on the output torque.

As it is shown in Fig. 13, the previsions coming from the linear stiffness model are not in accordance with the experimentation. In

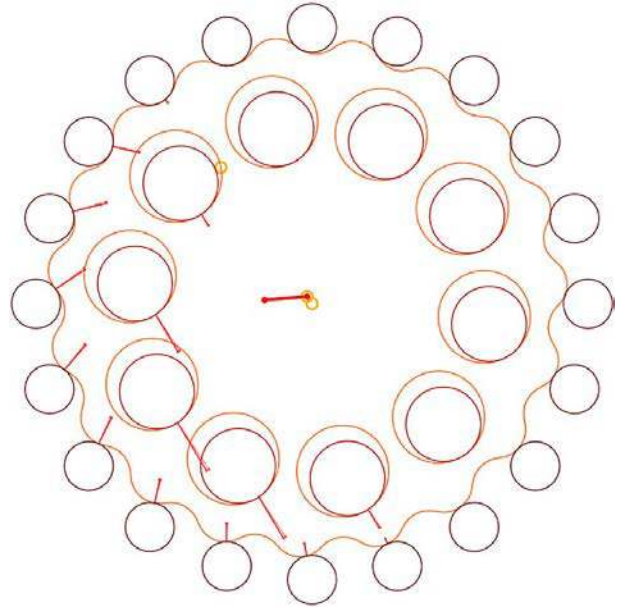


Fig. 12 Instant of simulations with rigid bodies model with the normal forces exchanged between cycloidal plate and rollers/housing pins/input shaft and the point of convergence of the normal forces exchanged with housing pins

agreement with the theory of contacts, the model of elasticity is non-linear. Several contacts introduce non-linear stiffness (input shaft and cycloidal disc, housing pins and cycloidal disc, output rollers, and cycloidal disc). The chosen model is based on empirical Palmgren equation model [20,21], for the contact between two cylinders. For each contact, the stiffness can be formulated as follows:

$$F = 8,06 \cdot 10^4 l^{8/9} \delta^{10/9} \quad (46)$$

where F is the contact force, l is the contact length, and δ is the normal displacement. So, we can formulate the contact stiffness as

$$F = k y_1^{10/9} \quad (47)$$

But the different contacts do not occur in the same time, so the contact between disc and pins, for example, can be modeled as shown in Fig. 14.

So, this contact can be mobilized as follows:

$$F = k \sum_{i=0}^n (y - y_i)^{10/9} \simeq k_{cy} y^p \quad (48)$$

With p factor more important than 10/9, in the case of the Fig. 14, p is greater than 2.

For easier computation, this function is reversed to define the load according to the displacement and approximated (fitting method) by a non-linear stiffness:

$$F = k_{cy} y_1 |y_1|^{p-1} \quad (49)$$

To take into account in this stiffness all the contacts, the p factor was identified from the experimental results and is equal to 2.35. This stiffness could be also computed with FEM as proposed in Refs. [15,16].

The simulations with the previous non-linear model are in accordance with measurements as Fig. 15 shows. The simulated displacements (Fig. 16) are in accordance with expected real displacements (not measured). As observed on the test bench, the more the load increases, the more the efficiency goes up as well.

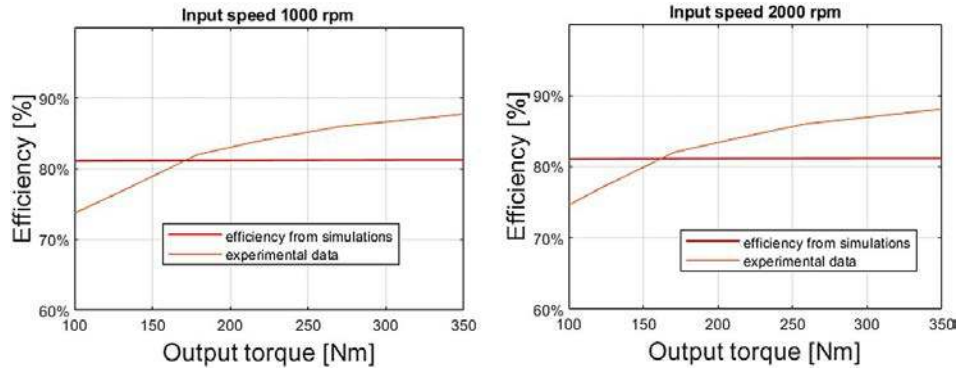


Fig. 13 Efficiency with the linear model ($p = 1$) at two different speeds with $k_{cy} = 10^9 \text{ N m}^{-1}$

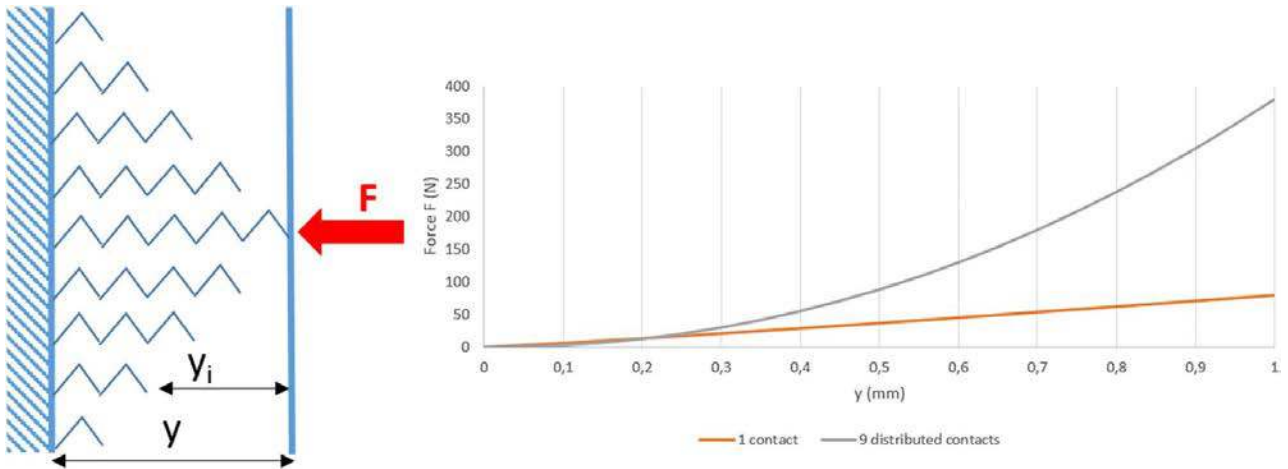


Fig. 14 Contact law for several pin with distributed loads

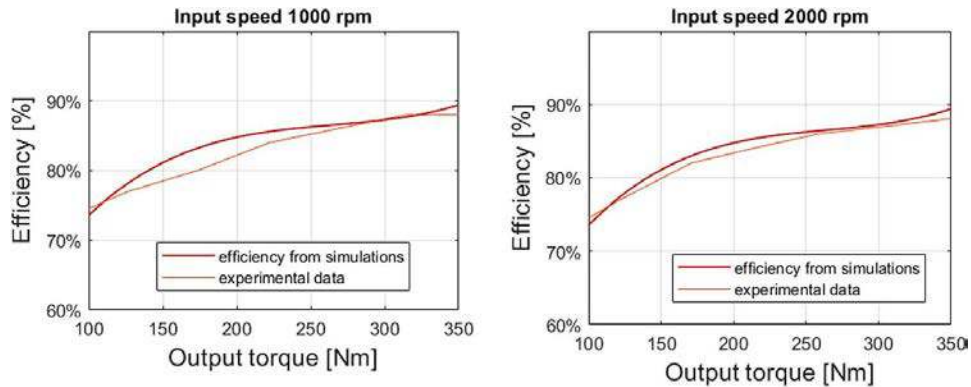


Fig. 15 Efficiency with the non-linear model ($p = 2.35$) at two different speeds with $k_{cy} = 1.5 \times 10^{10} \frac{\text{N}}{\text{m}^{2.35}}$

This phenomenon is the direct consequence of non-linear contact dynamics with the cycloidal disk.

7 Conclusions

A new model for cycloidal reducers is proposed. This model is based on kinematics and dynamics of rigid bodies and a non-linear stiffness. In this model, the elasticity effects are all condensed between input shaft and cycloidal disk.

The presented parametric reduced order model has allowed to have a quick model to fit to a physical cycloidal drive device. Then, from

this model, this method which requests light computational device and low time calculation, a wide parameter study can be performed to find the best optimized design regarding the initial one. This method is well adapted to industrial cycloidal drive.

As the experimentation and simulations show, the input speed has a negligible impact on the efficiency. The efficiency depends more on deformations linked to the normal load rather than on the sliding velocity. The efficiency of the cycloid drive rises with the increase of load. For small loads, it is almost linear and increases very fast, but for higher loads, the efficiency curve bends and grows more slowly.

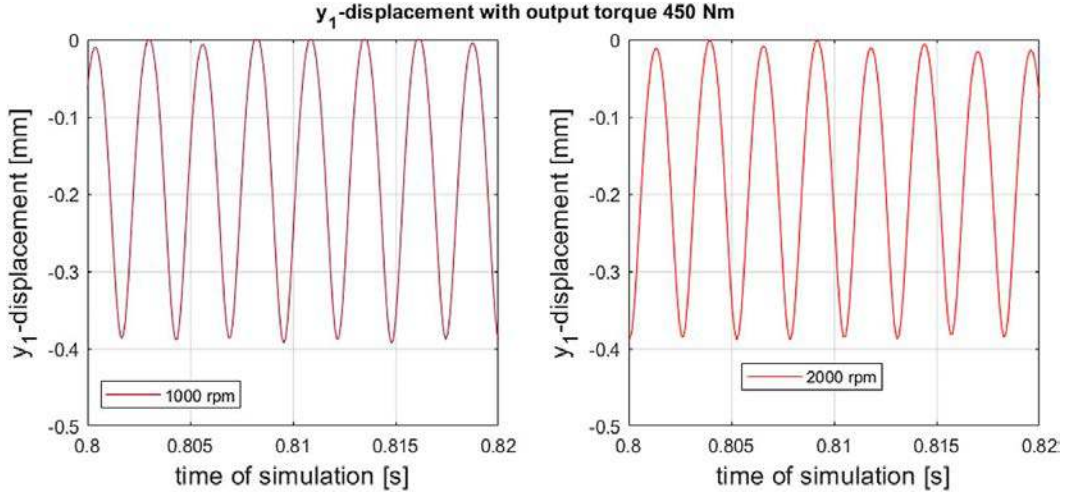


Fig. 16 Simulations results to evaluate the displacements with the non-linear model ($\rho = 2.35$) at two different speed with $k_{cy} = 1.5 \times 10^{10} \frac{N}{m^{2.35}}$

It has been shown that this shape of efficiency curve can be simulated by introducing non-linear stiffness into the model.

More generally, this work shows that a kinematic model with rigid bodies is not the representative of real phenomena and efficiency. The elasticity of solids in contact influences the efficiency. According to contact models, contact stiffness is non-linear, and the non-linearity depends on the shape of solids in contact which explains and justifies the trends of efficiency observed experimentally.

The proposed model is currently used for the design of new cycloid drives with an expected optimal efficiency. New and complementary models based on the finite element method are in development in order to identify the non-linear elasticity of contacts from the geometric specifications of cycloidal gearbox.

Nomenclature

- e = eccentricity
- i = gearbox ratio
- p = exponent of non-linearity
- k_{cy} = non-linear stiffness constant
- m_{cy} = cycloidal plate's mass
- y_1 = contact stiffness mobility parameter

- C_s = output constant load (torque)
- I_{zz} = disc's moment of inertia (around the main its axis)
- K_c = amplitude factor of forces exchanged between output rollers and disc
- K_s = amplitude factor of forces exchanged between housing pins and disc
- M_{C_i} = net torque exchanged between disc and pins
- M_{S_j} = net torque exchanged between disc and rollers
- C_{X_i}, C_{Y_i} = components of the forces exchanged between disc and pins
- E_x, E_y = component action on input shaft
- S_{X_j}, S_{Y_j} = components of the forces exchanged between disc and rollers
- T_{in}, T_{out} = shafts torque

Greek Symbols

- μ_E, μ_P, μ_S = friction coefficients between disc and input shaft, disc and housing pins, disc and output rollers
- φ = angular position of input shaft
- ϕ_2 = angular position on cycloidal plate
- $\omega_{in}, \omega_{out}$ = shafts speed

Appendix A: Parameters of Simulation

The following table summarizes all the main input parameters introduced:

Main geometrical reducer's features and dynamic parameters			
Cycloidal disc		Housing	
Symbol and description	Value	Symbol and description	Value
z_1 number of teeth	19	z_2 number of housing pins	20
r_1 primitive radius	91.2 mm	r_c housing pins radius	8.5 mm
x correction coefficient	0,38	r_2 pins distribution radius	96.0 mm
e_0 eccentricity	3.0 mm		
Output rollers		Dynamic parameters	
Symbol and description	Value	Symbol and description	Value
R_s roller distribution radius	62.0 mm	m_{cy} cycloidal disc mass	1.27 kg
N_c number of output rollers	10	μ_p housing pins friction coefficient	0.05
r_c output rollers radius	13.0 mm	μ_s output rollers friction coefficient	0.05
		μ_E bearing friction coefficient	0.005

The default value in the simulations ($\mu=0.05$) is suggested by the literature in the case of contact between steel ad steel with a lubricating film and bodies in mutual rolling.

Appendix B: Experimental Values of Efficiency

In order to show an example of the most relevant measures (directly measured and indirectly obtained) that we have focused on, detailed experimental data obtained with the input speed equal to 1000 rpm are given in the following table:

Viscosity, mm ² /s	Oil temp., °C	n_{in} , rpm	n_{out} , rpm	Speed ratio, –	T_{in} , Nm	T_{out} , Nm	η , –
42.1	33	1001	52.7	19.00	3.01	30.7	0.54
41.1	34.4	1001	52.7	19.00	6.11	83.2	0.72
44.4	32.5	1001	52.7	19.00	9.02	131.9	0.77
45.0	32.1	1001	52.7	19.00	11.45	178.9	0.82
44.1	32.6	1001	52.7	19.00	13.70	219.8	0.84
44.2	32.6	1001	52.7	19.00	16.66	271.1	0.86
43.0	33.3	1001	52.7	19.00	19.07	316.9	0.87
42.2	33.7	1001	52.7	19.00	21.58	361.9	0.88
42.0	33.9	1001	52.7	19.00	24.14	408.2	0.89
41.9	33.9	1001	52.7	19.00	26.67	450.5	0.89

References

- [1] Mackic, T., Blagojevic, M., Babic, Z., and Kostic, N., 2013, "Influence of Design Parameters on Cyclo Drive Efficiency," *J. Balkan Tribol. Assoc.*, **19**(4), pp. 167–179.
- [2] Blagojevic, M., Kocic, N., Marjanovic, M., Stojanovic, B., Dordevic, Z., Ivanovic, L., and Marjanovic, N., 2012, "Influence of the Friction on the Cycloidal Speed Reducer Efficiency," *J. Balkan Tribol. Assoc.*, **18**(2), pp. 217–227.
- [3] Blagojevic, M., Nikolic-Stanojevic, V., Marjanovic, N., and Veljovic, L., 2006, "Analysis of Cycloid Drive Dynamic Behavior," *Sci. Tech. Rev.*, **LIV**(1), pp. 23–29.
- [4] Shin, J.-H., and Kwon, S.-M., 2006, "On the Lobe Profile Design in a Cycloid Reducer Using Instant Velocity Center," *Mech. Mach. Theory.*, **41**(4), pp. 167–179.
- [5] Barone, S., Borgianni, L., and Forte, P., 2004, "Evaluation of the Effect of Misalignment and Profile Modification in Face Gear Drive by a Finite Element Meshing Simulation," *ASME J. Mech. Des.*, **126**(5), pp. 916–924.
- [6] Chen, B., Zhong, H., Liu, J., Li, C., and Fang, T., 2012, "Generation and Investigation of a New Cycloid Drive With Double Contact," *Mech. Mach. Theory.*, **49**(Mar.), pp. 270–283.
- [7] Hwang, Y.-W., and Hsieh, C.-F., 2007, "Determination of Surface Singularities of a Cycloidal Gear Drive With Inner Meshing," *Math. Comput. Model.*, **45**(4), pp. 340–354.
- [8] Sun, X., Han, L., and Wang, J., 2019, "Tooth Modification and Loaded Tooth Contact Analysis of China Bearing Reducer," *P I Mech. Eng. C-J. Mec.*
- [9] Borislavov, B., Borisov, I., and Panchev, V., 2012, Design of a Planetary Cyclo Drive Speed Reducer, Geometry, Element Analyses, Dissertation,
- [10] Larsson, E., 2013, "Optimising a Cyclo Drive," Ph.D. thesis, Lund University and Borg Warne, Sweden.
- [11] Malhotra, S., and Parameswaran, M., 1983, "Analysis of a Cycloid Speed Reducer," *Mech. Mach. Theory.*, **18**(6), pp. 491–499.
- [12] Olejarczyk, K., Wikto, M., and Kołodziejczyk, K., 2019, "The Cycloidal Gearbox Efficiency for Different Types of Bearings-Sleeves vs. Needle Bearings," *P I Mech. Eng. C-J. Mec.*
- [13] Gorla, C., Davoli, P., Rosa, F., Longoni, C., Chiozzi, F., and Samaran, A., 2008, "Theoretical and Experimental Analysis of a Cycloidal Speed Reducer," *ASME J. Mech. Des.*, **130**(11), p. 112604.
- [14] Hsieh, C.-F., and Fuentes-Aznar, A., 2019, "Performance Prediction Method of Cycloidal Speed Reducers," *J. Brazilian Soc. Mech. Sci. Eng.*, **41**(4), p. 186.
- [15] Sensinger, J., 2006, "Unified Approach to Cycloid Drive Profile, Stress, and Efficiency Optimization," *ASME J. Mech. Des.*, **132**(2), pp. 916–924.
- [16] Xu, L., and Yang, Y., 2016, "Dynamic Modeling and Contact Analysis of a Cycloid-Pin Gear Mechanism with a Turning Arm Cylindrical Roller Bearing," *Mech. Mach. Theory.*, **104**(Oct.), pp. 327–349.
- [17] Hsieh, C., 2014, "Dynamics Analysis of Cycloidal Speed Reducers With Pinwheel and Nonpinwheel Designs," *ASME J. Mech. Des.*, **139**(9), p. 091008.
- [18] Huang, C., and Tsai, S., 2017, "A Study on Loaded Tooth Contact Analysis of a Cycloid Planetary Gear Reducer Considering Friction and Bearing Roller Stiffness," *J. Adv. Mech. Des. Syst. Manuf.*, **11**(6), pp. 11–23.
- [19] Li, X., Li, C., Wang, Y., Chen, B., and Limand, T. C., 2017, "Analysis of a Cycloid Speed Reducer Considering Tooth Profile Modification and Clearance-Fit Output Mechanism," *ASME J. Mech. Des.*, **139**(3), p. 033303.
- [20] Harris, T., 2006, *Rolling Bearing Analysis*, Wiley-Interscience Publication, New York.
- [21] Palmgren, A., 1959, *Ball and Roller Bearing Engineering*, SKF Industries, Inc, Philadelphia.